Carbohydrate Polymers 117 (2015) 83–90

Contents lists available at ScienceDirect

Carbohydrate Polymers

journal homepage: www.elsevier.com/locate/carbpol

Starch and cellulose nanocrystals together into thermoplastic starch bionanocomposites

Kizkitza González [a], Aloña Retegi [a], Alba González [b], Arantxa Eceiza [a], Nagore Gabilondo [a,*]

[a] Materials + Technologies' Group, Department of Chemical and Environmental Engineering, Polytechnic School, University of the Basque Country, Pza. Europa 1, 20018 Donostia-San Sebastián, Spain

[b] POLYMAT, Department of Polymer Science and Technology, Faculty of Chemistry, University of the Basque Country, PO Box 1072, 20080 Donostia-San Sebastián, Spain

ARTICLE INFO

Article history:
Received 14 March 2014
Received in revised form
11 September 2014
Accepted 12 September 2014
Available online 28 September 2014

Keywords:
Bionanocomposite
Thermoplastic starch
Polysaccharide nanocrystals
Morphology
Thermal, mechanical and barrier properties

ABSTRACT

In the present work, thermoplastic maize starch based bionanocomposites were prepared as transparent films, plasticized with 35% of glycerol and reinforced with both waxy starch (WSNC) and cellulose nanocrystals (CNC), previously extracted by acidic hydrolysis. The influence of the nanofiller content was evaluated at 1 wt.%, 2.5 wt.% and 5 wt.% of WSNC. The effect of adding the two different nanoparticles at 1 wt.% was also investigated. As determined by tensile measurements, mechanical properties were improved at any composition of WSNC. Water vapour permeance values maintained constant, whereas barrier properties to oxygen reduced in a 70%, indicating the effectiveness of hydrogen bonding at the interphase. The use of CNC or CNC and WSNC upgraded mechanical results, but no significant differences in barrier properties were obtained. A homogeneous distribution of the nanofillers was demonstrated by atomic force microscopy, and a shift of the two relaxation peaks to higher temperatures was detected by dynamic mechanical analysis.

1. Introduction

Starch, in form of its thermoplastic derivate (TPS), has been revealed as an appropriate candidate to be employed as substitute of synthetic polymers traditionally used for packaging, due to its versatility, availability, biodegradability, processability and low cost. Starch is a hydrophilic semicrystalline biopolymer stored in form of granules in the native state that consists of a mixture of two glycosidic macromolecules, i.e. amylose and amylopectin (Carvalho, 2008; Le Corre, Bras, & Dufresne, 2010). Amylose is a linear polysaccharide made up of (1-4) α-D-glycopyranose, whereas amylopectin is a highly branched macromolecule composed of both α(1-4) and α(1-6) glycopyranosyl linkages (García, Ribba, Dufresne, Aranguren, & Goyanes, 2011; Le Corre et al., 2010). The arrangement of the two polymers in form of alternant amorphous and crystalline rings lead to the final semicrystalline granules, being amylopectin the main responsible of the crystalline character (Le Corre et al., 2010).

Actually, starch is not a real thermoplastic polymer, but can be processed after its gelatinization by mixing with enough water and/or plasticizers (Angellier, Molina-Boisseau, Dole, & Dufresne, 2006; Carvalho, 2008; García et al., 2011; Viguié, Molina-Boisseau, & Dufresne, 2007). The crystallinity of starch granules disappears during the gelatinization process, and at the end, an amorphous material is obtained (Carvalho, 2008). In most investigations the plasticization of the material is carried out by casting a dispersion of starch with glycerol (Angellier et al., 2006; Bertuzzi, Vidaurre, Armada, & Gottifredi, 2007; Carvalho, 2008; García, Ribba, Dufresne, Aranguren, & Goyanes, 2009; Yan, Hou, Guo, & Dong, 2012), but other water soluble plasticizers such as sorbitol, xylitol, maltitol, urea or ethylene glycol have been also used (Abdorreza, Cheng, & Karim, 2011; Da Róz, Carvalho, Gandini, & Curvelo, 2006; Viguié et al., 2007; Wang, Cheng, & Zhu, 2014). Attempting to reduce the undesired well-known sensitivity to moisture and temperature of TPS, several strategies have been developed in the literature (Averous, Moro, Dole, & Fringant, 2000; Xie, Pollet, Halley, & Avérous, 2013).

Bionanocomposites have already been identified as useful materials for achieving the mentioned objectives. The addition of different nanocrystals to the starch based matrix, would lead to both mechanical and barrier properties improvement of the material. In this context, nanoclays and polysaccharide derived

* Corresponding author. Tel.: +34 943017231/+34 943017162; fax: +34 943017200.
E-mail address: nagore.gabilondo@ehu.es (N. Gabilondo).

http://dx.doi.org/10.1016/j.carbpol.2014.09.055
0144-8617/

nanocrystals have been tried in the most recent researches (Angellier et al., 2006; García et al., 2011; Xie et al., 2013). Actually, a large amount of work has been published mainly with cellulose whiskers and, in a less extent, chitin or starch nanocrystals (Wang, Tian, & Zhang, 2010). Disordered amorphous domains of natural polysaccharides can be removed by acid hydrolysis (Habibi, Lucia, & Rojas, 2010; Lin, Huang, Chang, Anderson, & Yu, 2011; Lin, Huang, & Dufresne, 2012), under controlled conditions, leaving the crystalline regions intact (Lin et al., 2012), and thus, nanometrical high crystallinity particles are obtained. However, little work has been reported using different polysaccharide nanocrystals simultaneously (Wang et al., 2010). Nanocrystals extracted from different sources have a variety of geometrical structures (Wang et al., 2010), and thus, they are supposed to have their own properties and applications as reinforcing agent. While cellulose nanocrystals were found to be rod like or fibrillar (Angellier, Molina-Boisseau, Belgacem, & Dufresne, 2005; Lin et al., 2012; Wang et al., 2010), starch nanocrystals isolated from waxy maize presented a platelet like morphology (Habibi et al., 2010; Lin et al., 2012; Saralegi et al., 2013) and would be preferred for barrier properties enhancement (LeCorre, Bras, & Dufresne, 2012). However, the expected improvement of mechanical, thermal or barrier properties by the addition of nanocrystals extracted from different origins would depend on both a correct dispersion and the generation of an active interphase nanoreinforcement/matrix.

One of the most common applications of TPS based biocomposites is their use as films in food packaging products. A critical issue in food packaging is that of migration of certain components and vapour and gases permeability (Duncan, 2011). Many authors have investigated the improvement of water vapour and oxygen permeability in reinforced TPS materials (Bertuzzi et al., 2007; Chivrac, Angellier-Coussy, Guillard, Pollet, & Avérous, 2010; García et al., 2009; Kelnar, Kaprálková, Brozová, Hromádkova, 2013; Xie et al., 2013). The barriers to oxygen and water vapour are two essential properties to consider in starch-based material because these can deteriorate food properties. The gas transport trough the film depends hardly on the diffusivity. Tortuous pathways for gas molecules diffusion, created by dispersed nanocrystals, increase molecule migration and consequently limit permeability (Le Corre et al., 2010). It is important to take into account that permeability is also affected by solubility, which is related with the chemical nature and crystallinity of the polymer, and sample homogeneity. Polysaccharides, such as TPS, are well known to be effective barrier materials to oxygen transport, whereas they present high water permeability values (Bertuzzi et al., 2007).

The main objective of the present work was to investigate the effect of different contents of waxy maize starch nanocrystals on a normal maize starch matrix plasticized by glycerol. In addition, the influence of using together nanocrystals from similar chemical nature with different geometries, i.e. waxy maize starch and cellulose nanocrystals, was studied in order to investigate possible synergistic effects. The thermoplastic starch was obtained by casting process and both polysaccharide nanocrystals were extracted by acid hydrolysis. The nanometrical dimensions and the degree of crystallinity of nanocrystals were investigated. Resulting nanobiocomposites were characterized in terms of thermal stability, mechanical properties and barrier properties.

2. Experimental

2.1. Materials

Waxy maize starch and normal corn starch were purchased from Sigma-Aldrich and glycerol (99% purity) from Panreac. The former, almost completely amylopectin, was employed for the preparation of starch nanocrystals (WSNC) and the latter, with higher content of amylose, nearly 25%, was used for the preparation of thermoplastic starch (TPS).

2.2. Preparation of waxy starch nanocrystals (WSNC)

The preparation of the waxy starch nanocrystals (WSNC) was carried out by acidic hydrolysis according to the method described elsewhere (Angellier, Choisnard, Molina-Boisseau, Ozil, & Dufresne, 2004; García et al., 2011). 36.725 g of waxy starch maize were mixed with 250 ml of H_2SO_4 solution (3.16 M) during 5 days at 40 °C under continuous magnetic stirring. The suspension was washed and centrifuged with distilled water until neutralization. The obtained nanocrystals were stored at 4 °C after adding some drops of chloroform.

2.3. Preparation of cellulose nanocrystals (CNC)

The extraction of the crystalline part of cellulose was also performed by acidic hydrolysis as explained by Saralegi et al. (2013). 5 g of microcrystalline cellulose (MCC) were treated with a H_2SO_4 64 wt.% aqueous solution. The reaction was completed during 30 min at 45 °C with continuous stirring. After that, the acidity was reduced by centrifugation (twice, 4500 rpm, 20 min) and the precipitate was neutralized by dialysis (4–5 days). Finally, the suspension was ultrasonicated for 15 min.

2.4. Preparation of thermoplastic starch (TPS)

The thermoplastic starch and the subsequent nanocomposites were obtained by casting based on the method described by Angellier et al. (2006) with some modifications. A mixture of 3.58 g of normal maize starch, 1.93 g of glycerol and 35 g of distilled water was gelatinized at 90 °C with continuous stirring until viscosity increased (about 20 min). After that, the material was spread into glass petri and dried in an oven at 55 °C for 2 h (CSg35). For the preparation of nanocomposites, the desired amount of nanocrystals was added, after their previous dispersion in distilled water by ultrasonication. In order to avoid the gelatinization of starch nanocrystals, the mixture was cooled down below 50 °C before adding the nanoreinforcements. Thereafter, the processing was carried out as described above (CSg35 + wt.%). All the samples were stored at 43% relative humidity (RH) with a K_2CO_3 saturated solution for two weeks before all characterization tests. A glycerol content of 35 wt.% was used for all samples, i.e. relative to the starch plus water mixture weight. The nanofiller content was relative to the starch plus glycerol weight and WSNC or CNC contents were relative to the total nanocrystals weight. The samples were named as CSg35 plus the nanocrystals content, followed by the WSNC and/or CNC proportion. Bionanocomposites are referred hereafter as shown in Table 1.

Table 1
Compositions of obtained bionanocomposites.

	Nanocrystal (wt.%)	WSNC (wt.%)	CNC (wt.%)
CSg35	0	0	0
CSg35 + 1 (100/0)	1	100	0
CSg35 + 1 (50/50)	1	50	50
CSg35 + 1 (0/100)	1	0	100
CSg35 + 2.5	2.5	100	0
CSg35 + 5	5	100	0

2.5. Characterization

2.5.1. Atomic force microscopy (AFM)

Atomic force microscopy (AFM) measurements were performed in tapping mode using a Veeco Multimode scanning probe microscope equipped with a Nanoscope IIIa Controller. All measurements were recorded using TESP type silicon tips having a resonance frequency of approximately 340 kHz and a cantilever spring constant about 40 N/m. Both nanocrystals and cryofractured surfaces of nanocomposites were analyzed.

2.5.2. Optical microscopy (OM)

The study of the gelatinization process, i.e. the transformation of starch into a thermoplastic and amorphous material, was performed by optical microscopy, analyzing the change of the crystalline structure and the evolution of the birefringence. The analyses were carried out with a Nicon Eclipse E600 instrument in reflectance and with a magnification of ×500.

2.5.3. X-ray diffraction (XRD)

All samples were submitted to X-ray radiation using an Xpert diffractometer, 40 kV, 40 mA. Scattered radiation was detected in the angular range 1–40° (2θ). The XRD curves were used to determine the crystallinity percentage of WSNC and CNC. For WSNC an appropriate method is not so widely established, for this reason the crystallinity degree was determined by the ratio of the crystalline area to the total area (Jivan, Madadlou, & Yarmand, 2013; Rosa et al., 2010).

$$\text{WSNC, Crystallinity percentage } (\%) = \frac{\text{Area under the peaks}}{\text{Total area}} \times 100$$

Crystallinity for CNC was calculated according to the method described in literature (Kargarzadeh et al., 2012; Segal, Creely, Martin, & Conrad, 1959).

$$\text{CNC, Crystallinity percentage } (\%) = \frac{I_{002} - I_{am}}{I_{002}} \times 100$$

where I_{002} is the peak intensity of the (0 0 2) crystallographic plane (Kargarzadeh et al., 2012), i.e. the intensity peak near $2\theta = 22.5°$ (Lin, Huang, Chang, Feng, & Yu, 2011) and I_{am} is the intensity scattered by the amorphous part of the sample measured around $2\theta = 18.0°$ (Kargarzadeh et al., 2012).

2.5.4. Thermogravimetric analysis (TGA)

Thermogravimetric analysis was carried out in order to investigate the degradation process of all nanocomposites using a Mettler Toledo TGA-SDTA 851 instrument. The samples were heated from room temperature to 800 °C, with a heating rate of 10 °C min^{-1} and under nitrogen.

2.5.5. Tensile tests

The mechanical behaviour of the nanocomposites was analyzed using a MTS Insight 10 instrument. Dumbbell shaped specimens 5 mm wide and 15 mm long (L_0) were used. The initial gap between jaws was adjusted to 22 mm.

2.5.6. Dynamic mechanical analysis (DMA)

Dynamic mechanical analysis was carried out using an Eplexor 100N instrument from Gabo Qualimeter. The specimen was a rectangular strip ($25 \times 3 \times 0.2$ mm^3), it was subjected to a 0.05% constant strain and the setup measured the stored modulus E' the loss modulus E'' and the ratio between the two components ($\tan\delta = E''/E'$). Measurements were performed at 1 Hz, working from −100 °C to 150 °C with a heating rate of 2 °C min^{-1}.

2.5.7. Water vapour permeability (WVP)

Water vapour permeation experiments were performed at 25 °C on a gravimetric cell in which a small amount of liquid water was sealed by a membrane. The cell was put on a balance with a readability of 10–5 g, and the weight loss of the cell, solely due to the permeation of the water vapour through the membrane, was followed by means of a computer connected to the balance.

2.5.8. Oxygen permeability (OP)

The measurements were carried out using a MOCON OX-TRAN Model 2/21 gas permeability tester in accordance with the ASTM standard D3985. The permeability of samples was tested at 760 mmHg, HR = 50% and 23 °C.

3. Results and discussion

3.1. Characterization of polysaccharide nanocrystals

Geometrical structure and dimensions at the nanoscale of the nanocrystals were studied by Atomic force microscopy (AFM) (Fig. 1a and b). Assuming the cylindrical shape of CNC (Saralegi et al., 2013) mean diameter values were obtained by the evaluation of AFM height profiles. For WSNC, since they trend to agglomerate, less single nanocrystals were possible to measure. Nanometrical dimensions of both waxy starch and cellulose nanocrystals were confirmed. Waxy starch nanoparticles were found to be platelet like, with 28.2 ± 7.4 nm in width and 35 ± 7.9 nm in length. Cellulose nanocrystals presented the typical fibril like geometry with 9.1 ± 2.6 nm in diameter and 150.6 ± 29.1 nm in length. These results agreed with those obtained in literature (Angellier et al., 2005; Wang et al., 2010; Saralegi et al., 2013).

X-ray diffraction (XRD) measurements were carried out in order to observe the crystalline polymorphism for each type of nanocrystal (Fig. 1c). XRD pattern of WSNC showed the typical A-type polymorphism with two peaks of low intensity located at $2\theta = 10.1°$ and $2\theta = 11.5°$, a peak at $2\theta = 15.2°$ of higher intensity, a double peak near $2\theta = 17.3°/18.1°$ and an intense peak at 23.2°. Cellulose nanocrystals pattern exhibited strong peaks at $2\theta = 14.5°$, $2\theta = 16.8°$ and $2\theta = 22.7°$ associated to the typical cellulose I crystalline structure. As explained by Lin et al. (2012), the crystallinity degree of polysaccharide nanocrystals should be 100%. However, disorder or amorphous domains cannot be completely removed by hydrolysis, leading to a lower crystallinity degree. Following the method described elsewhere (Jivan et al., 2013; Rosa et al., 2010), a crystallinity percentage of 22.8% for WSNC was established. Besides, according to the method reported previously (Kargarzadeh et al., 2012; Segal et al., 1959) a crystallinity percentage of 83.6% was calculated for CNC. Other authors (Buléon, Colonna, Planchot, & Ball, 1998; Lin et al., 2012) determined similar values for CNC obtained from MCC (54–88%), but higher crystallinity degree percentages for WSNC (38–48%). Differences could be related to the different extraction protocol employed, along with the method used for calculating crystallinity degrees (Jivan et al., 2013; Rosa et al., 2010). However, even if the crystallinity percent of the WSNC could be affected slightly by the calculation method, the results for CNC were, as expected, significantly higher. Attending to AFM and XRD results, it was concluded that the employed hydrolysis methods were satisfactory.

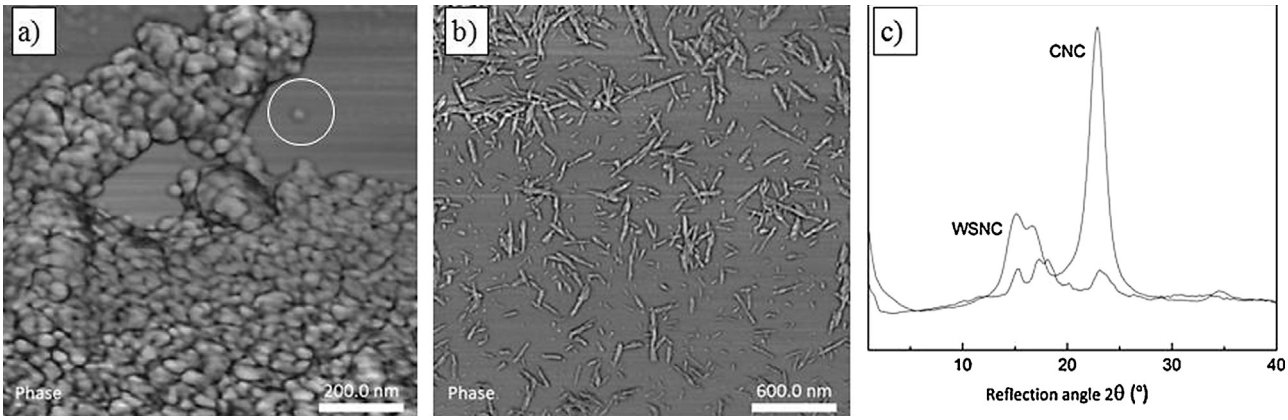

Fig. 1. Characterization of polysaccharide nanoreinforcements: AFM images of extracted (a) WSNC and (b) CNC and (c) X-ray diffraction patterns for nanocrystals.

3.2. Characterization of bionanocomposites

3.2.1. Influence of the WSNC content

Prior to the preparation of the bionanocomposites, the gelatinization of the matrix was optimized following the disappearance of the birefringence by optical microscopy. The effect of the nanoreinforcement content on thermal, mechanical and barrier properties was investigated for nanocomposites of TPS reinforced with WSNC. XRD results for the TPS/WSNC bionanocomposites showed that the A-type polymorphism pattern of the native normal maize starch was replaced by a typical broad peak centred at $2\theta = 19.6^\circ$ in the case of the amorphous thermoplastic derivative. However, as WSNC content increased, peaks associated to the nanoreinforcements were progressively detected, in concordance with results published previously in literature (Angellier et al., 2006).

Thermogravimetric measurements were carried out to assess the thermal decomposition of all nanocomposites (Fig. 2). Unplasticized normal maize starch showed a single degradation step at 300 °C. On the contrary, the thermal decomposition process for as-prepared nanocomposites occurs in three main steps (García et al., 2009, 2011). The first step (25–100 °C) related to the loss of sorbed humidity, the second one (100–200 °C) associated to the decomposition of the glycerol-rich phase and the last one (below 340 °C) due to the oxidation of the partially decomposed starch. The degradation stability decrease of the bionanocomposites may be maximized by the affinity between glycerol and waxy starch nanocrystals. Acidic sulphate ester groups attached to waxy starch nanocrystals surface during the extraction seemed to act as catalyzers of the thermal decomposition, resulting in a clear decrease of degradation temperature for nanocomposites compared with that for the unfilled matrix. At the same time, the final char percentage increased with the nanoreinforcement content.

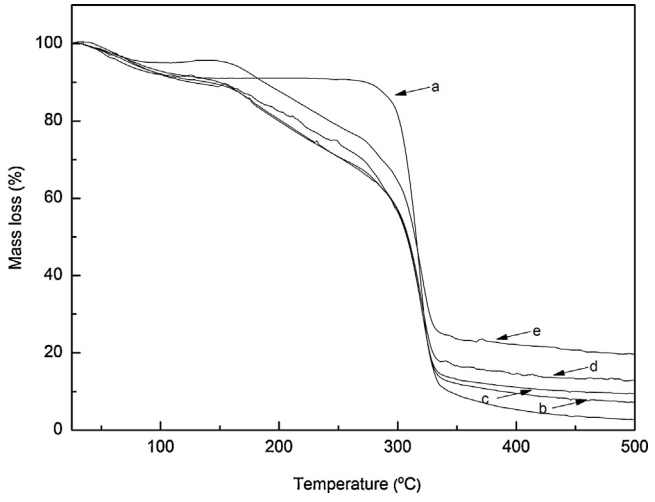

Fig. 2. TGA curves for (a) Normal maize starch (b) CSg35, (c) CSg35 + 1 (100/0), (d) CSg35 + 2.5 and (e) CSg35 + 5.

The mechanical properties of bionanocomposites reinforced with different contents of WSNC were determined by means of tensile tests. Obtained results are collected in Table 2. The addition of WSNC resulted in a significant improvement of the mechanical properties of the TPS. Indeed, the Young's Modulus increased from 2.5 MPa for the plasticized starch to 7.5 MPa for the bionanocomposites, the tensile strength was improved in a 70%, with only a slight variation in deformability at break. Due to the identical chemical nature of the matrix and the nanofiller, a good affinity between both components was expected, allowing strong TPS/WSNC hydrogen bonding at the interfaces and the subsequent favourable reinforcing effect. However, it is worth noting that mechanical properties of bionanocomposites were not further improved from 2.5 wt.% to 5 wt.% of WSNC content. The reinforcing effect of starch nanocrystals is generally ascribed to the formation of a hydrogen bonded percolating filler network above a given starch content corresponding to the percolation threshold (Le Corre et al., 2010). Our results seemed to indicate that starch nanocrystals were correctly dispersed in an effective percolated network up to a 2.5 wt.% of reinforcement.

Gas and vapour permeability of polymeric materials is independent of film thickness in ideal systems. However, TPS based films present non-ideal behaviour with increasing permeability values proportionally to the film thickness providing an increasing resistance to mass transfer trough the film (Bertuzzi et al., 2007). In our study such deviation was detected, being the relationship between thickness and water vapour permeability almost linear ($R^2 > 0.98$). For this reason, both for water vapour and oxygen mass transfer, the calculation of permeance values was preferred. Obtained results are collected in Table 2. Nanocomposites development respond to the hypothesis that nanometric particles incorporated into a polymeric matrix would generate a tortuous path for vapour or gas and, consequently, the diffusive component of the permeability would decrease. Besides the diffusion, polymers barrier properties depends on other factors as polarity and structural features of polymeric side chains, hydrogen bonding characteristics, molecular weight and polydispersity, degree of branching or cross-linking, processing methodology and degree of crystallinity (Duncan, 2011). Platelet-like starch nanocrystals are supposed to have good attributes in the improvement of barrier properties but, according to water vapour permeability, due to their hydrophilic nature, low crystallinity and agglomeration

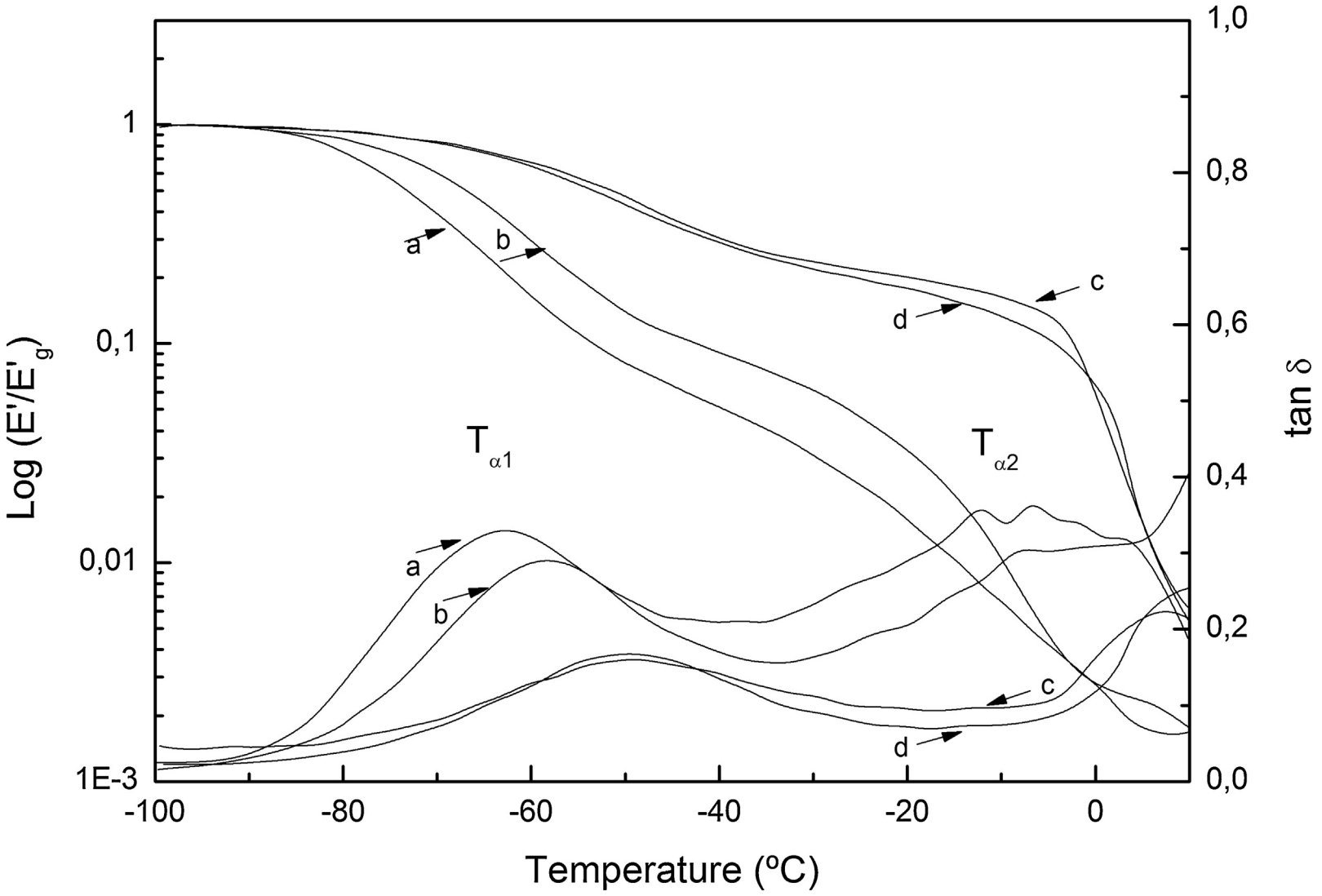

Fig. 3. Evolution of E' and tan δ with temperature for (a) CSg35, (b) CSg35 + 1 (100/0), (c) CSg35 + 2.5, (d) CSg35 + 5.

Table 2
Tensile properties and water vapour and oxygen permeance values for plasticized starch and TPS-WSNC nanocomposites.

	Young's modulus (MPa)	Strain at break (%)	Tensile strength (MPa)	Water vapour permeance ($kg\,m^{-2}\,s\,Pa) \times 10^{10}$	Oxygen permeance ($cm^3\,m^{-2}$ day atm)
CSg35	2.5 ± 0.9	52.7 ± 9.4	1.0 ± 0.2	56.2 ± 2.0	22.7 ± 3.9
CSg35 + 1 (100/0)	5.8 ± 0.9	48.8 ± 24.4	1.7 ± 0.4	66.7 ± 4.5	26.9 ± 1.6
CSg35 + 2.5	7.4 ± 1.1	41.8 ± 8.7	1.6 ± 0.3	57.3 ± 3.8	15.5 ± 4.7
CSg35 + 5	7.5 ± 1.1	47.9 ± 10.3	1.6 ± 0.1	57.3 ± 1.4	7.7 ± 1.5

opposite conclusions have been reported for their nanocomposites (Le Corre et al., 2010). In our particular investigation, whereas water permeance values were not reduced by the addition of starch nanocrystals, oxygen permeance was significantly improved for 2.5 wt.% and 5 wt.% of WSNC contents. Bertuzzi et al. (2007) and Forssell, Lahtinen, Lahelin, and Myllärinen (2002) correlated these results with sorbed water-starch interactions that are closely related with water transport phenomena. These interactions were not generated with oxygen molecules, and that is why oxygen permeance values were improved. As it could be noted, whereas CSg35 and CSg35 + 1 (100/0) presented similar permeance to O_2, it was reduced to $7.7 \pm 1.5\,cm^3\,m^{-2}$ day atm, for 5 wt.% of WSNC content, suggesting that the presence of a minimum concentration was necessary to create an actual tortuous pathway. This significant improvement for higher WSNC contents suggests that those were effectively dispersed in the TPS matrix and points out the close interface adhesion between nanocrystals and matrix. The viscoelastic behaviour of the bionanocomposites was assessed by Dynamic mechanical analysis (Fig. 3). Two-step modulus drop relative to the tan δ peaks temperatures near −60 °C ($T_{\alpha 1}$) and −20 °C ($T_{\alpha 2}$) was observed. García et al. (2009) attributed them to the glycerol-rich phase and starch-rich phase relaxation temperatures, respectively. As it can be noted, the addition of 1 wt.% of WSNC resulted in a significant shift of $T_{\alpha 1}$ which is related to an increase in the rigidity of the glycerol-rich phase. As the WSNC content increased, the peak shifted to temperatures close to −50 °C. At the same time, $T_{\alpha 2}$ also moved to higher temperatures mainly in bionanocomposites filled with 2.5 wt.% and 5 wt.%, revealing that a good dispersion of the nanocrystals was achieved and the reinforcement effect was homogeneously distributed in both phases. Thus, DMA results were in good agreement with results obtained from both tensile and permeance measurements.

3.2.2. *Influence of nanocrystals' origin on bionanocomposites*

The influence of nanocrystal nature was analysed when WSNC and CNC were combined together in TPS. 1 wt.% composition was chosen in order to better analysing any synergistic effect resulting from the simultaneous action of both nanocrystals. This assumption lays on the fact that the platelet shape of WSNC would enhance barrier properties improvement (Duncan, 2011), whereas rod-like high crystalline CNC would contribute in a higher extent to the mechanical reinforcement as they present higher aspect ratio, reducing the percolation threshold. Four different WSNC–CNC nanocrystal contents were studied (Table 1).

Mechanical behaviour was evaluated by means of tensile tests and obtained results are shown in Table 3. Some remarkable changes were detected when cellulose or waxy starch nanocrystals were added into the matrix. First, higher values of Modulus were obtained for CNC filled nanocomposites at the same composition. This finding agrees with the fact that higher mechanical reinforcement would be achieved by using high aspect ratio rod-like nanocrystals (Flauzino Neto, Silvério, Dantas, & Pasquini, 2013; Wang et al., 2010). The opposite effect was detected for deformation at break, as it was reduced in a larger extent. It is worth noting that the Young's Modulus was considerably improved up to 12.0 MPa for the CSg35 + 1 (50/50) system, i.e. the one where WSNC and CNC were combined. Wang et al. (2010) obtained similar results using waterborne polyurethane as matrix. As they explained, the combination of both nanometric reinforcements would lead to a much jammed hydrogen bonding network between nanofiller and the matrix. However, taking into account the variability of the measurements, in our opinion these findings should be corroborated in further investigations.

Table 3 summarized the results of water vapour and oxygen permeance obtained for the bionanocomposites containing WSNC and/or CNC. Large nanoparticle aspect ratios are required to reduce the gas permeability by an appreciable degree (Duncan, 2011). Attending to the results, it could be concluded that the incorporation of CNC to the bionanocomposite did not result in any improvement of the barrier properties. On one hand, water vapour permeability seemed to be again governed by the strong chemical affinity of the material with water molecules. On the other hand, the higher aspect ratio and crystallinity of CNC did not reduce the oxygen permeance values (only slight decrease is noting for the CSg35 + 1 (0/100) sample), revealing that in studied polysaccharide-based films, barrier properties improvement was more correlated to the nanofiller content than to the origin of it. Nanocomposites reinforced with waxy starch and cellulose nanocrystals showed the same rheological behaviour in comparison with films reinforced only with WSNC (Fig. 4). Indeed, almost identical DMA curves were obtained with the characteristic two-step modulus drop related to the two different phases. The addition of polysaccharide nanocrystals resulted in higher relaxation temperatures (T_α) values whatever its origin was. This effect could be ascribed to the fact that both starch and cellulose nanocrystals interacted strongly with the glycerol-rich phase. However, a remarkable higher shift of the $T_{\alpha 1}$ value to higher temperatures was observed for bionanocompostes containing WSNC. On the contrary, $T_{\alpha 2}$ maintained almost constant. These results confirmed the interaction between glycerol-rich phase domains and the reinforcing nanocrystals, especially with waxy starch nanocrystals.

AFM was used for the morphological characterization of the cryofractured nanocomposite samples. Fig. 5a and b shows the obtained images for CSg35 + 1 (100/0) and CSg35 + 1 (0/100),

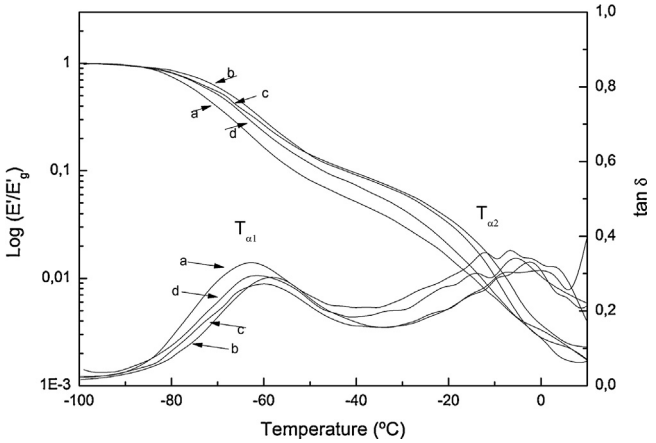

Fig. 4. Evolution of the E' and tan δ with temperature for (a) CSg35, (b) CSg35 + 1 (100/0), (c) CSg35 + 1 (50/50), (d) CSg35 + 1 (0/100).

Table 3
Tensile properties and water vapour and oxygen permeance values for TPS and TPS + WSNC/CNC.

	Young's modulus (MPa)	Strain at break (%)	Tensile strength (MPa)	Water vapour permeance ($kg\,m^{-2}\,s\,Pa) \times 10^{10}$	Oxygen permeance ($cm^3\,m^{-2}$ day atm)
CSg35	2.5 ± 0.9	52.7 ± 9.4	1.0 ± 0.2	56.2 ± 2.0	22.7 ± 3.9
CSg35 + 1 (100/0)	5.8 ± 0.9	48.8 ± 24.4	1.7 ± 0.4	66.7 ± 4.5	26.9 ± 1.6
CSg35 + 1 (50/50)	12.0 ± 2.0	41.7 ± 4.2	1.6 ± 0.1	54.2 ± 1.1	26.6 ± 1.9
CSg35 + 1 (0/100)	8.5 ± 2.2	41.9 ± 8.5	1.5 ± 0.2	57.9 ± 2.7	22.1 ± 1.1

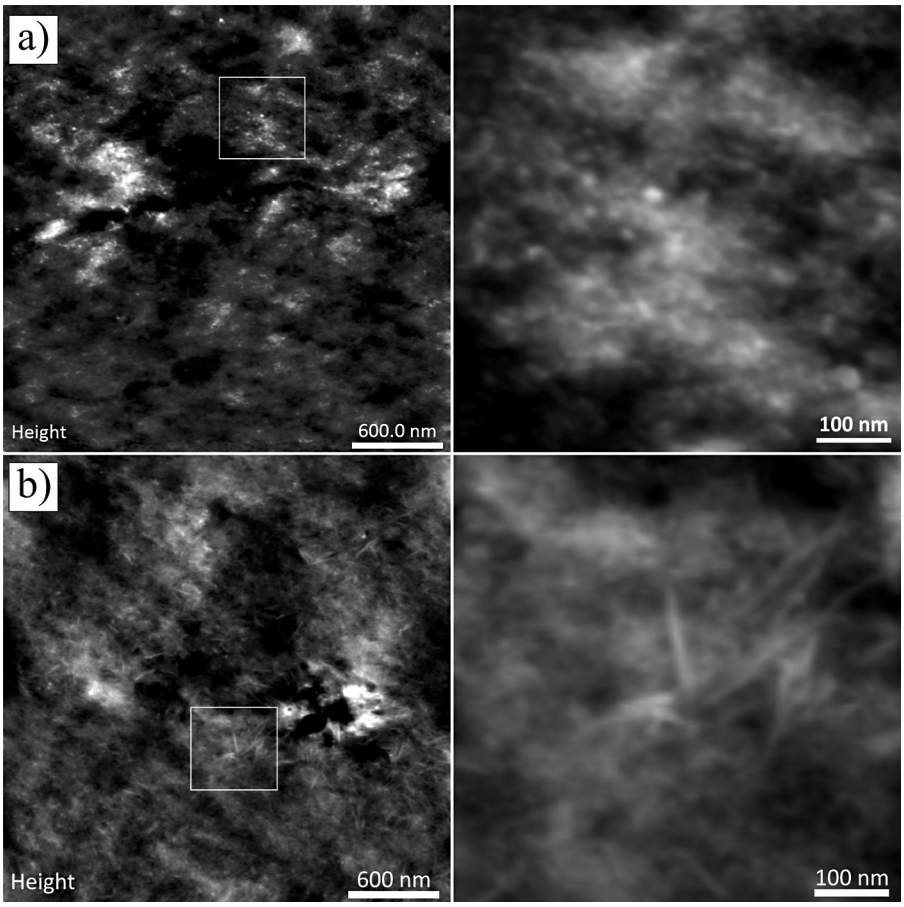

Fig. 5. AFM height images of (a) CSg35 + 1 (100/0) and (b) CSg35 + 1 (0/100).

respectively. In case of the CSg35 + 1 (100/0) sample, starch nanocrystals were observed as ill-defined nanoparticles due to their extremely reduced dimensions. However, focusing on the amplified image where the dimensions of the nanofillers were possible to evaluate individually, it could be concluded that nanocrystals were correctly dispersed, in good agreement with the conclusions extracted previously.

4. Conclusions

AFM and XRD results demonstrate that the acid hydrolysis protocols used to obtain both waxy starch and cellulose nanocrystals were satisfactory. Also TOM and XRD corroborated that method employed in the gelatinization to produce thermoplastic starch and resulting nanocomposites was successful. TGA results defined that the thermal degradation of nanocomposites occurs in three main steps. Also was demonstrated that the addition of NC reduces the thermal stability of all samples. The mechanical properties and oxygen permeance values of the TPS-WSNC nanocomposites are clearly higher than those of the unfilled matrix. The addition of 2.5 wt.% of WSNC to the starch thermoplastic matrix represents a significant improvement of the mechanical and oxygen permeance properties. Mechanical properties were also enhanced with the addition of CNC for CSg35 + 1 (50/50) and CSg35 + 1 (0/100) samples, due to the reinforcement ability of CNC. However, DMA curves show an increased of the relaxation temperature since the addition of nanocrystals result in a stronger affinity between glycerol and NC phases.

Acknowledgments

Financial support from the Basque Country Government in the frame of Saiotek S-PE12UN036 and Grupos Consolidados (IT-776-13) and from the University of the Basque Country (UPV/EHU) in the frame of EHUA12/19 is gratefully acknowledged. Technical and human support provided by SGIker (UPV/EHU, MINECO, GV/EJ, ERDF and ESF) is also gratefully acknowledged.

References

Abdorreza, M. N., Cheng, L. H., & Karim, A. A. (2011). Effects of plasticizers on thermal properties and heat sealability of sago starch films. *Food Hydrocolloids*, *25*, 56–60.

Angellier, H., Choisnard, L., Molina-Boisseau, S., Ozil, P., & Dufresne, A. (2004). Optimization of the preparation of aqueous suspensions of waxy maize starch nanocrystals using a response surface methodology. *Biomacromolecules*, *5*, 1545–1551.

Angellier, H., Molina-Boisseau, S., Belgacem, M. N., & Dufresne, A. (2005). Surface chemical modification of waxy maize starch nanocrystals. *Langmuir*, *21*, 2425–2433.

Angellier, H., Molina-Boisseau, S., Dole, P., & Dufresne, A. (2006). Thermoplastic starch–waxy maize starch nanocrystals nanocomposites. *Biomacromolecules*, *7*(2), 531–539.

Averous, L., Moro, L., Dole, P., & Fringant, C. (2000). Properties of thermoplastic blends: starch–polycaprolactone. *Polymer*, *41*(11), 4157–4167.

Bertuzzi, M. A., Vidaurre, E. F. C., Armada, M., & Gottifredi, J. C. (2007). Water vapor permeability of edible starch based films. *Journal of Food Engineering*, *80*, 972–978.

Buléon, A., Colonna, P., Planchot, V., & Ball, S. (1998). Starch granules: Structure and biosynthesis. *International Journal of Biological Macromolecules*, *23*, 85–112.

Carvalho, A. J. F. (2008). Starch: Major sources, properties and applications as thermoplastic materials. In M. N. Belgacem, & A. Gandini (Eds.), *Monomers, polymers and composites from renewable resources* (pp. 321–342). The Publisher is Elsevier Ltd. ISBN: 978-0-08-045316-3.

Chivrac, F., Angellier-Coussy, H., Guillard, V., Pollet, E., & Averous, L. (2010). How does water diffuse in starch/montmorillonite nano-biocomposite materials? *Carbohydrate Polymers*, *82*(1), 128–135.

Da Róz, A., Carvalho, A., Gandini, A., & Curvelo, A. (2006). The effects of plasticizers on thermoplastic starch compositions obtained by melt processing. *Carbohydrate Polymers*, *63*, 417–424.

Duncan, V. T. (2011). Applications of nanotechnology in food packaging and food safety: Barrier materials, antimicrobials and sensors. *Journal of Colloid and Interface Science*, *363*, 1–24.

Flauzino Neto, W. P., Silvério, H. A., Dantas, N. O., & Pasquini, D. (2013). Extraction and characterization of cellulose nanocrystals from agro-industrial residue-soy hulls. *Industrial Crops and Products*, *42*, 480–488.

Forssell, P., Lahtinen, R., Lahelin, M., & Myllärinen, P. (2002). Oxygen permeability of amylose and amylopectin films. *Carbohydrate Polymers*, *47*, 125–129.

García, N. L., Ribba, L., Dufresne, A., Aranguren, M., & Goyanes, S. (2009). Physicomechanical properties of biodegradable starch nanocomposites. *Macromolecular Materials and Engineering*, *294*, 169–177.

García, N. L., Ribba, L., Dufresne, A., Aranguren, M., & Goyanes, S. (2011). Effect of glycerol on the morphology of nanocomposites made from thermoplastic starch and starch nanocrystals. *Carbohydrate Polymers*, *84*, 203–210.

Habibi, Y., Lucia, L. A., & Rojas, O. J. (2010). Cellulose nanocrystals: Chemistry, self-assembly, and applications. *Chemical Reviews*, *110*(6), 3479–3500.

Jivan, M. J., Madadlou, A., & Yarmand, M. (2013). An attempt to cast light into starch nanocrystals preparation and cross-linking. *Food Chemistry*, *141*, 1661–1666.

Kargarzadeh, H., Ahmad, I., Abdullah, I., Dufresne, A., Zainudin, S. Y., & Sheltami, R. M. (2012). Effects of hydrolysis conditions on the morphology, crystallinity, and thermal stability of cellulose nanocrystals extracted from kenaf bast fibers. *Cellulose*, *19*(3), 855–866.

Kelnar, I., Kaprálková, L., Brozová, L., Hromádková, J., & Kotek, J. (2013). Effect of chitosan on the behaviour of the wheat B-starch nanocomposite. *Industrial Crops and Products*, *46*, 186–190.

Le Corre, D., Bras, J., & Dufresne, A. (2010). Starch nanoparticles: A review. *Biomacromolecules*, *11*, 1139–1153.

LeCorre, D., Bras, J., & Dufresne, A. (2012). Influence of native starch's properties on starch nanocrystals thermal properties. *Carbohydrate Polymers*, *87*, 658–666.

Lin, N., Huang, J., Chang, P. R., Anderson, D. P., & Yu, J. (2011). Preparation, modification, and application of starch nanocrystals in nanomaterials: A review. *Journal of Nanomaterials*, http://dx.doi.org/10.1155/2011/573687

Lin, N., Huang, J., Chang, P. R., Feng, L., & Yu, J. (2011). Effect of polysaccharide nanocrystals on structure, properties, and drug release kinetics of alginate-based microspheres. *Colloids and Surfaces B: Biointerfaces*, *85*, 270–279.

Lin, N., Huang, J., & Dufresne, A. (2012). Preparation, properties and applications of polysaccharide nanocrystals in advanced functional nanomaterials: A review. *Nanoscale*, *4*(11), 3274–3294.

Rosa, M. F., Medeiros, E. S., Malmonge, J. A., Gregorski, K. S., Wood, D. F., Mattoso, L. H. C., et al. (2010). Cellulose nanowhiskers from coconut husk fibers: Effect of preparation conditions on their thermal and morphological behaviour. *Carbohydrate Polymers*, *81*(1), 83–92.

Saralegi, A., Rueda, L., Martin, L., Arbelaiz, A., Eceiza, A., & Corcuera, M. A. (2013). From elastomeric to rigid polyurethane/cellulose nanocrystal bionanocomposites. *Composites Science and Technology*, *88*, 39–47.

Segal, L., Creely, J. J., Martin, A. E., Jr., & Conrad, C. M. (1959). An empirical method for estimating the degree of crystallinity of native cellulose using the X-ray diffractometer. *Textile Research Journal*, *29*(10), 786–794.

Viguié, J., Molina-Boisseau, S., & Dufresne, A. (2007). Processing and characterization of waxy maize starch films plasticized by sorbitol and reinforced with starch nanocrystals. *Macromolecular Bioscience*, *7*(11), 1206–1216.

Wang, J.-L., Cheng, F., & Zhu, P-X. (2014). Structure and properties of urea-plasticized starch films with different urea contents. *Carbohydrate Polymers*, *101*, 1109–1115.

Wang, Y. X., Tian, H., & Zhang, L. (2010). Role of starch nanocrystals and cellulose whiskers in synergistic reinforcement of waterborne polyurethane. *Carbohydrate Polymers*, *80*, 665–671.

Xie, F., Pollet, E., Halley, P. J., & Avérous, L. (2013). Starch-based nano-biocomposites. *Progress in Polymer Science*, *38*, 1590–1628.

Yan, Q., Hou, H., Guo, P., & Dong, H. (2012). Effects of extrusion and glycerol content on properties of oxidized and acetylated corn starch-based films. *Carbohydrate Polymers*, *87*, 707–712.